POAC'25
St. John's, Newfoundland and Labrador, Canada

Proceedings of the 28th International Conference on Port and Ocean Engineering under Arctic Conditions
Jul 13-17, 2025
St. John's, Newfoundland and Labrador
Canada

# Experimental study on uniaxial compressive strength of Summer Arctic sea ice under impact loading

Shuang Yu[1,2], Xiaodong Chen[1,2], Shunying Ji[1,2], Qinglin Duan[1,2]
[1] (Dalian University of Technology, Dalian, China)
[2] (State Key Laboratory of Structural Analysis, Optimization and CAE Software for Industrial Equipment, Dalian, China)

## ABSTRACT

Collisions between polar ships and sea ice are often associated with high strain rates. Understanding the dynamic mechanical properties of sea ice is crucial for the design and safety of ship structures. To investigate the uniaxial compressive strength of sea ice under impact loading, a drop-weight impact device was used to conduct uniaxial compression tests on sea ice samples collected during China's 13th Arctic Expedition in the melting season. A high-speed camera recorded the failure process during impact. The tests were conducted at an ice temperature of -5°C, with strain rates ranging from 4.2 $s^{-1}$ to 23 $s^{-1}$. To provide a comparative analysis, Quasi-static uniaxial compression tests were also performed at the same temperature, with strain rates between $10^{-5}$ $s^{-1}$ and $10^{-2}$ $s^{-1}$.The results show that the compressive strength of sea ice is similar in magnitude under quasi-static and impact loading in the strain rate range of the test. However, the trends differ significantly. Under quasi-static loading, the compressive strength first increases and then decreases with higher strain rates. Under impact loading, it increases continuously with strain rate. An empirical formula relating dynamic compressive strength to strain rate was developed based on data fitting. It was observed that the failure of sea ice under impact loading was caused by the combined effects of local compression, splitting failure and crushing failure. Further relationship between energy absorption during failure and strain rate was also identified.

KEY WORDS: Arctic sea ice; Impact tests; Uni-axial compressive strength; Failure mode; Energy

## INTRODUCTION

As global warming continues, Arctic sea ice is melting at an accelerated rate(Wang et al.,2024). This leads to significant changes in its physical and mechanical properties.

Understanding how sea ice behaves under impact loading during the Arctic melt season is essential for designing ice-resistant marine structures in the region.

Many researchers have studied the dynamic mechanical properties of ice (Combescure et al., 2011; Pernas-Sánchez et al., 2015; Zhang et al., 2023; Franciska Müller et al., 2024). Most studies have focused on freshwater ice, while fewer have been conducted on sea ice. Jones(1997) used a uniaxial compression testing machine to study the strength of freshwater ice and low-salinity Baltic Sea ice. The tests were conducted at strain rates of $10^{-1}$ to $10^{1}$ $s^{-1}$, and the results showed that the compressive strength of both types of ice increased with the strain rate. Other researchers have used the Hopkinson bar method to study ice compressive strength at high strain rates. Kim and Keune(2007) found that ice compressive strength stayed nearly the same at an average of 19.7 MPa across the measured strain rate range(400~600 $s^{-1}$). In contrast, the studies by Shazly et al.(2009) and Wu and Prakash(2015) suggest that ice compressive strength increased with rising strain rates within their experimental range. Lian et al. (2017) used a high-speed testing machine and studied the uniaxial compressive strength of natural lake ice at strain rates of 0.4 to 10 $s^{-1}$. The results showed that the dynamic uniaxial compressive strength of lake ice shows positive strain-rate sensitivity.

To explore the compressive strength of sea ice under impact loading, this study conducted drop-weight impact tests on summer sea ice samples collected during the 13th Chinese Arctic Expedition. The tests changed different drop heights to achieve different strain rates. Quasi-static uniaxial compression tests were also performed for comparison.

## 1 Methods

This study investigates the compressive strength of Arctic summer sea ice collected during China's 13th Arctic Scientific Expedition. To determine the compressive strength at different strain rates, impact and quasi-static loading tests were performed using a specially developed drop-weight impact device and a portable testing machine. Due to limitations in field testing, both the impact and quasi-static uniaxial compression tests were completed in the laboratory four months after sample collection. As sea ice is an anisotropic material, its mechanical properties vary with the loading direction. In this test, forces were applied along the direction which was vertical in-situ.

### 1.1 Ice Samples

The collection of sea ice samples was completed during China's 13th Arctic Scientific Expedition. Based on ice conditions along the route, ice stations were established on floating ice floes accessible to the icebreaker. The sampling locations for the sea ice samples in this study are shown in Fig. 1. The sea ice samples for the impact tests were collected at Site 1 in the Chukchi Sea on August 13, 2023, while those for the quasi-static loading tests were collected at Site 2 in the central Arctic Ocean on September 2, 2023. At each ice station, a flat and even ice floe was selected as the sampling location. A Kovacs drill with a 90 cm diameter was used to extract ice cores for mechanical property testing. The drilled ice cores were sealed in core bags and stored in a low-temperature box, then transported to a laboratory in Dalian, China, under -20°C conditions. Before testing, the ice cores were cut into cylindrical samples 150 mm in height and 90 mm in diameter using a band saw. The collection and preparation of the sea ice samples are shown in Fig. 2. The processed sea ice samples were stored in a freezer at -5°C for about 24 hours to ensure uniform internal and external temperatures before the tests.

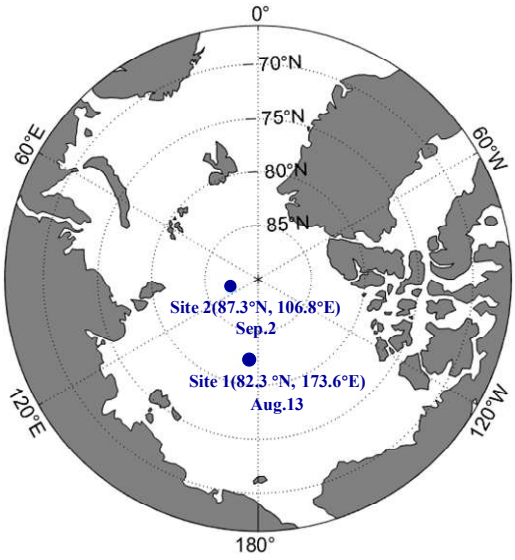


Fig.1 The sampling locations for the sea ice samples

Fig.2 The collection and preparation of the sea ice samples

### 1.2 Drop-weight impact device

This test was performed using a specially developed drop hammer impact testing device, depicted in Fig. 3. To apply different strain rates, the device adjusts the hammer's drop height by moving a steel plate equipped with an electromagnet along the support rail. The drop hammer, with a mass of 34 kg, is released from heights between 7.5 cm and 115 cm to generate varying impact velocities. However, energy loss during the drop (e.g., due to air resistance and mechanical friction) reduces the actual impact velocity compared to the theoretical value derived from free-fall kinematics. A piezoelectric sensor (IEPE F1000E) with a 30 kN range and 1~10,000 Hz frequency response was mounted on the hammer's impact head, ensuring precise dynamic force measurements. During testing, load signals were recorded at 100 kHz. When the electromagnet was activated, the hammer dropped freely to impact the ice specimen. A high-speed camera, operating at 7500 fps with LED lighting, captured the sample's failure process and hammer motion, ensuring detailed ice fracture capture without affecting the sample temperature.

The mechanical properties of sea ice are closely linked to its physical properties. For each test, it is essential to measure parameters like salinity, density, and temperature of the sea ice.

Density is determined by directly measuring the sample's mass and volume. The sample's dimensions are measured using a vernier caliper to calculate its volume. An electronic balance is used to measure the mass of each sample segment, and density is then calculated. Salinity is determined by measuring the salinity of the meltwater from the fractured ice samples collected after the loading phase. These samples are placed in a container to melt, and the salinity of the resulting meltwater is measured. Temperature is measured after the test concludes by drilling a hole in the fractured ice sample and inserting a probe thermometer once the temperature stabilizes.

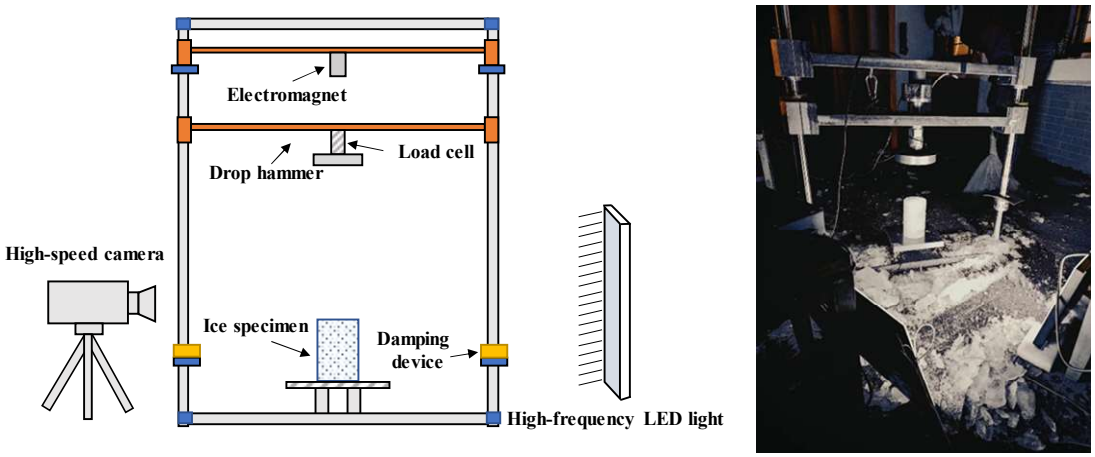


Fig.3 Drop-weight impact device

### 1.3 Portable testing machine

A portable testing machine was used as the loading device for the quasi-static uniaxial compression tests on sea ice. This machine is shown in Fig. 4. The upper part of the machine's loading area is fixed, while the lower part is driven by a servo cylinder to move the crossbeam. Equipped with a 30 kN load cell with an accuracy of ±0.1%, the machine is controlled by a numerical control system. This system drives the servo cylinder to achieve a constant loading speed of 0.001 to 1 mm/s. The strain rate for the quasi-static tests ranged from $10^{-6}$ to $10^{-2}$ $s^{-1}$. Similar to the impact tests, each test required measuring the physical properties of the sea ice samples.

Fig.4 The quasi-static uniaxial compression test of sea ice

### 1.4 Calculation of Experimental Parameters

During the test, the load cell recorded the load variation on the sea ice sample, generating a load-time curve. The uniaxial compressive strength of the sea ice $\sigma_c$ is calculated from the equation

$$\sigma_c = \frac{F_{\max}}{A} \tag{1}$$

where $F_{\max}$ is the maximum load in the load-time curve; and $A$ is the initial cross-sectional area of sea ice sample. The average deformation is expressed by the ratio between the platen displacement and initial sample length, and can be written as

$$\varepsilon_{nom} = \frac{d}{L} \tag{2}$$

where $\varepsilon_{nom}$ is the nominal strain; $d$ is the platen displacement; $L$ is the initial height of sea ice sample.

Here, we can define the nominal strain-rate as

$$\dot{\varepsilon}_{nom} = \frac{v}{L} \tag{3}$$

where $v$ is the velocity of the drop hammer in drop-weight impact test or the loading rate of portable testing machine, and the drop hammer speed is calculated based on the high - speed camera recordings; $L$ is the height of the sample. Due to energy loss during the drop hammer's fall, the impact velocity is calculated using high-speed camera recordings. A 30 mm thick indenter serves as the image calibration reference. The impact velocity is determined by tracking the position change of a reference point in each frame of the impact images. Fig.5 shows the calculation diagram for impact velocity.

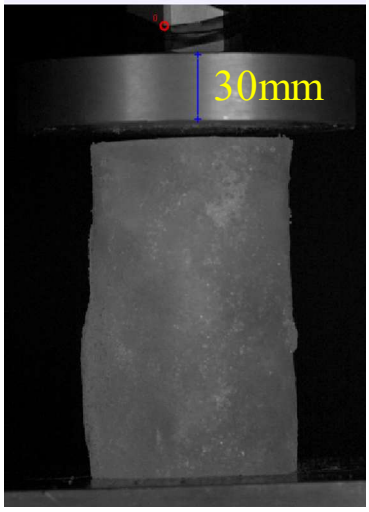


Fig.5 The calculation diagram for impact velocity

## 2 RESULTS& DISCUSSION

## 2.1 Physical properties

Sea ice is a complex material composed of solid ice, brine, gases, and various solid salts. Its growth is influenced by environmental factors such as temperature and ocean currents, resulting in non-uniform physical properties along its thickness. In this test, samples cut from the same ice core were labeled for identification. During uniaxial compression tests, the salinity and density of the samples were measured. The profiles of salinity and density across the ice floe from different locations are presented in Fig.6. The Arctic summer sea ice exhibits characteristics of low salinity and low density. The salinity and density profiles of sea ice from the two sampling locations exhibit similar trends of increasing with depth. This depth-dependent trend arises from elevated summer temperatures, which dissolve solid salts trapped in the ice at lower temperatures. The resulting brine pockets expand and connect to form "brine channels." Driven by gravity, the denser brine percolates downward, concentrating salt in deeper layers and increasing salinity and density with depth.

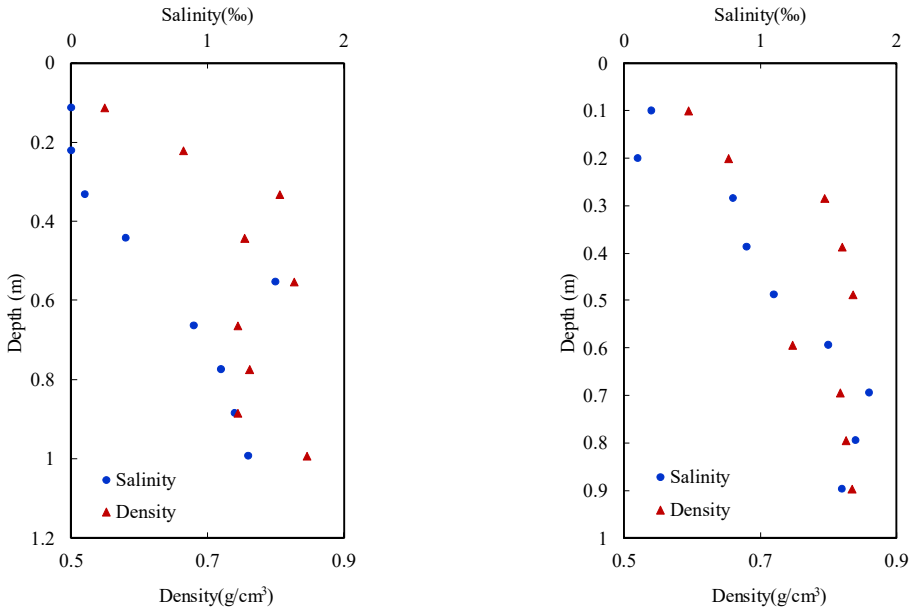


(a) The profiles of salinity and density across the ice floe from site 1

(b) The profiles of salinity and density across the ice floe from site 2

Fig.6 The profiles of salinity and density across the ice floe from different locations

## 2.2 The failure mode under impact loading

The failure process of sea ice samples can be divided into three stages: local compression, splitting, and crushing. Fig.7 shows failure images of sea ice samples at different strain rates. Initially, local compression occurs at the end of the sample in contact with the indenter, leading to stress concentration and the formation of initial cracks. These cracks then propagate vertically or at an angle, penetrating the entire sample and causing splitting. As compression continues, the number of vertical cracks increases, splitting the sample into multiple columnar fragments. Eventually, the sample undergoes crushing. Within the experimental strain rate range, the failure mode remains consistent. However, as the strain rate increases, the sample is broken into more small-sized fragments, indicating greater energy absorption during the failure process.

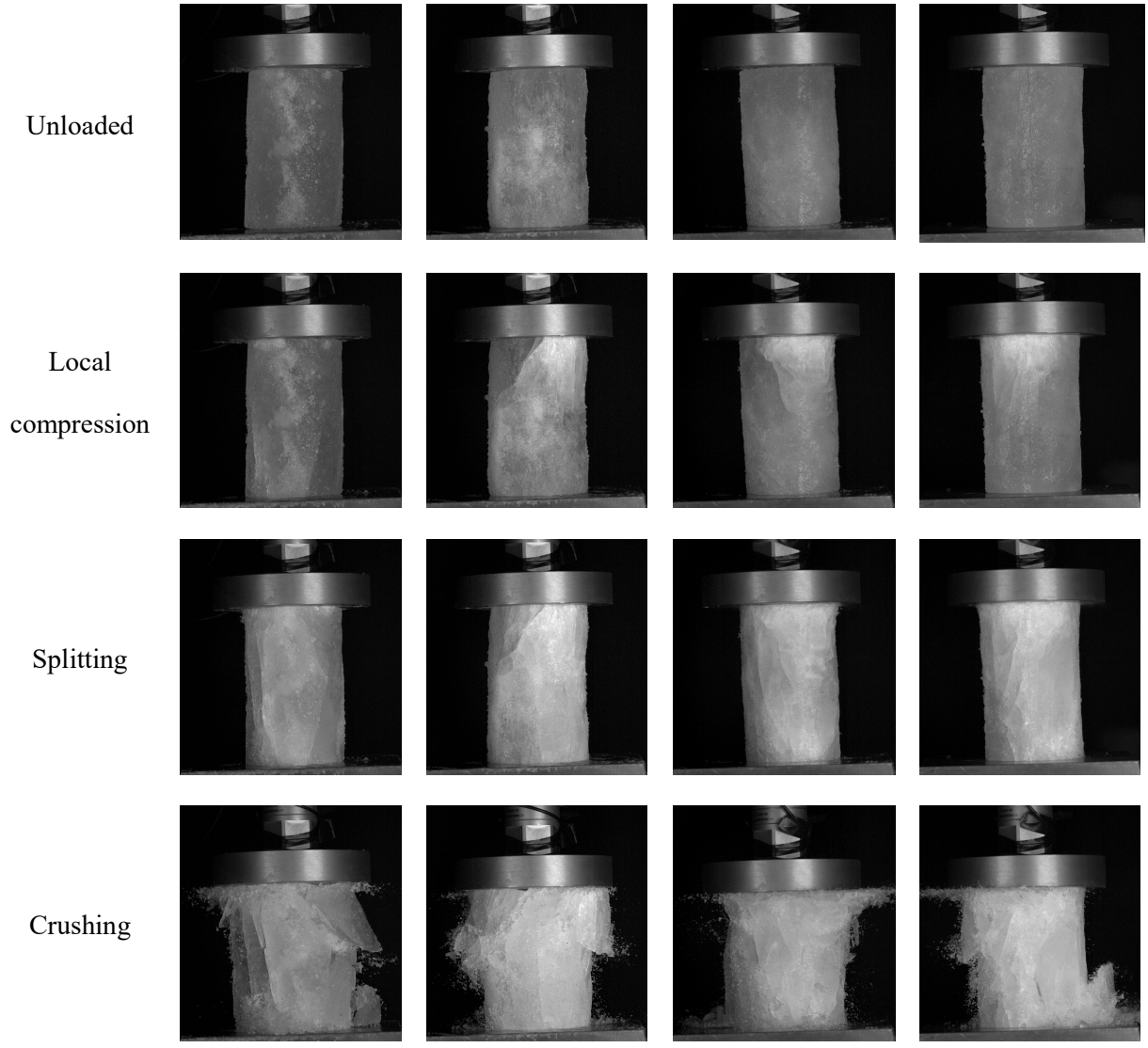


Fig.7 The failure mode of sea ice samples under impact loading

### 2.3 Stress-strain relationship

Fig. 8 presents the stress-strain curves of samples under the two loading modes. Under quasi-static loading, the failure process of sea ice samples mainly takes three forms: ductile failure, single-peak brittle failure, and multi-peak brittle failure. At low strain rates, the stress-strain curve increases and decreases smoothly, with no abrupt changes, indicating ductile behaviour of the sea-ice sample. As the strain rate increases, the stress of the sea ice sample drops to zero immediately after reaching the peak, showing a transition to brittle failure. At high strain rates, the stress curve shows multiple peaks, indicating the presence of multiple through cracks in the sea ice sample. Under impact loading, all samples exhibited brittle failure. During the impact failure process, the load may oscillate, but for all specimens, the load rises to its maximum value at the very beginning. Therefore, only the first cycle was selected for analysis in the stress-strain

curve. The stress-strain curve drops to zero rapidly after reaching the peak, and the peak stress increases with the strain rate.

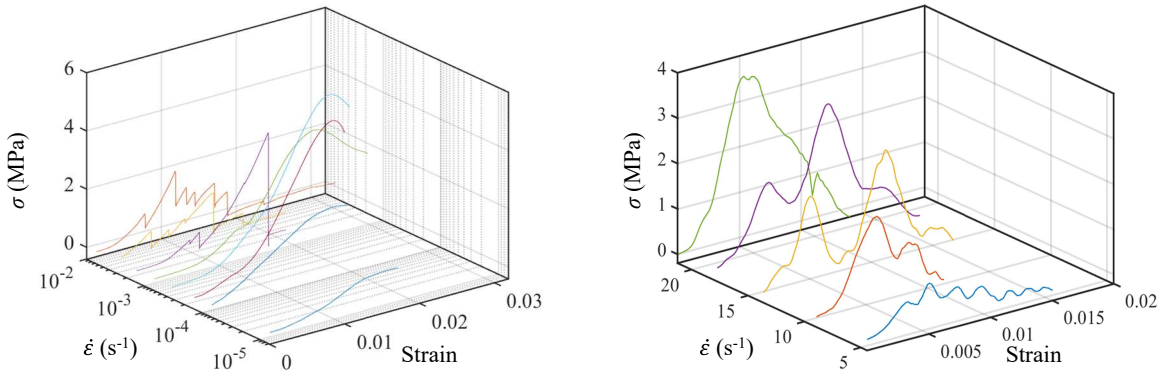


(a) Stress-strain curve of sea ice samples under quasi-static loading

(b) Stress-strain curve of sea ice samples under impact loading

Fig.8 Stress-strain curves of samples under two loading modes

### 2.4 Compressive strength versus strain rates

The compressive strength of sea ice displays a significant sensitivity to strain rate. Results of uniaxial compressive strength versus strain rates are shown in Fig.9. For quasi-static loading, which corresponds to strain rates ranging from $10^{-6}$ to $10^{-2}$ $s^{-1}$, the compressive strength varies between 0.46 MPa and 5.33 MPa. At low strain rates, sea ice shows good ductility. However, as the strain rate increases, the failure mode of sea ice shifts to brittleness. The compressive strength initially rises and then declines. When it comes to impact loading, represented by strain rates from 4.2 $s^{-1}$ to 23 $s^{-1}$, the compressive strength falls between 0.90 MPa and 4.74 MPa. In this case, the compressive strength increases gradually with the rising strain rate. Jones(1997) conducted tests on the compressive strength of Baltic Sea ice using a high-speed machine. A power-law function was employed to fit the relationship between compressive strength and strain rate:

$$\sigma_c = 6\dot{\varepsilon}^{0.19} \tag{4}$$

It is evident that Jones's test results are substantially higher than those presented in this paper. One contributing factor is that the sea ice sampled in this study was retrieved during the summer melt season, consequently containing more pores. Additionally, Jones's test was conducted at -10℃, a lower temperature than that in this paper. Given these factors, the compressive strength of sea ice in this study can be fitted with power-law function to establish a formula applicable to Arctic sea ice during the melt season:

$$\sigma_c = 0.54\dot{\varepsilon}^{0.53} (R^2 = 0.46) \tag{5}$$

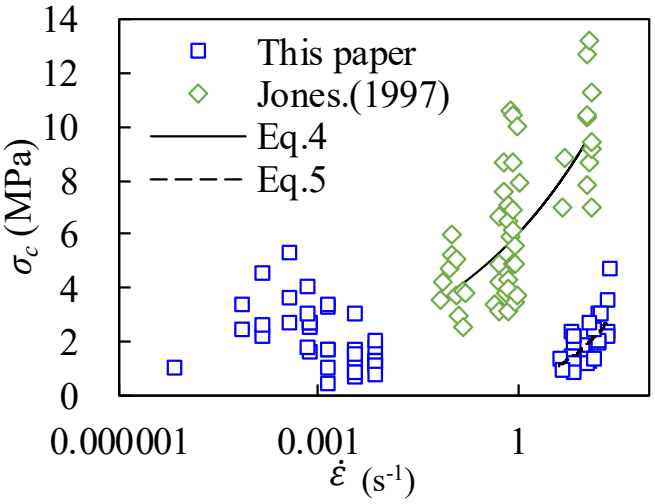


Fig.9 Results of uniaxial compressive strength versus strain rates

### 2.5 The energy absorption under impact loading

The energy absorption of sea ice samples is obtained by integrating the Force-displacement curve. Fig. 9(a) shows the energy calculation example for sample at 21.2 s$^{-1}$. The grey area under the blue curve represents the energy absorbed during failure. Fig. 10(b) reveals the positive relationship between the energy absorption of sea ice samples and the strain rate: higher strain rates result in greater energy absorption during sample failure.

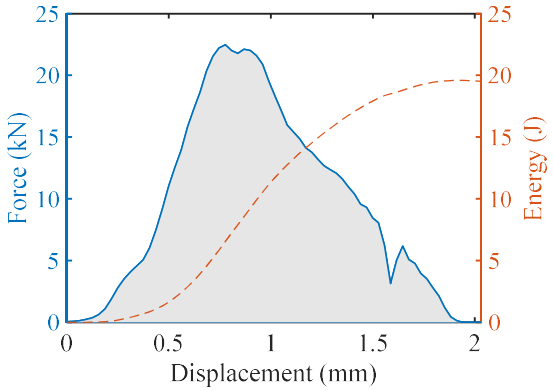


(a) The energy calculation example for sample at 21.2 s$^{-1}$

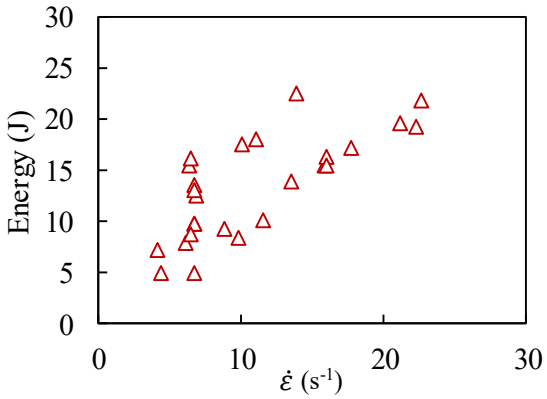


(b) Results of energy absorption versus strain rates

Fig.10 The energy absorption of sea ice samples under impact loading

## CONCLUSIONS

This study conducted quasi-static uniaxial compression tests and drop-weight impact tests on Arctic sea ice samples collected during China's 13th Arctic Scientific Expedition. The main conclusions are as follows:

- The Arctic sea ice during the melting season exhibited lower dynamic compressive strength due to melting. Under quasi-static loading, the compressive strength of the

sea ice ranged from 0.46 MPa to 5.3 MPa, while under impact loading, the compressive strength ranged from 0.90 MPa to 4.74 MPa.

- The failure of sea ice under impact loading was caused by the combined effects of local compression, splitting failure and crushing failure.
- Under quasi-static loading, the compressive strength first increased and then decreased with higher strain rates. Under impact loading, it increased continuously with strain rate. A power-law relationship was established based on experimental data under impact loading.
- Under impact loading, the energy absorbed during ice failure increased with rising strain rate.

## ACKNOWLEDGEMENTS

This research was supported by the National key research and development program (Grant No. 2024YFC2816403), National Natural Science Foundation of China (Grant Nos. 52101300,52192693, 52192690, 42176241), Social Development Science and Technology Project of Shanghai Science and Technology Innovation Plan (22DZ1204500) and Special Project of Ministry of Industry and In-formation Technology of China (Grand No. 2021-342).

## REFERENCES

Combescure, A., Chuzel-Marmot, Y., & Fabis, J. (2011). Experimental study of high-velocity impact and fracture of ice. *International Journal of Solids and Structures*, 48(20), 2779-2790.

Jones, S. J. (1997). High strain-rate compression tests on ice. *The Journal of Physical Chemistry B*, 101(32), 6099-6101.

Kim, H., & Keune, J. N. (2007). Compressive strength of ice at impact strain rates. *Journal of Materials Science*, 42, 2802-2806.

Lian, J., Ouyang, Q., Zhao, X., Liu, F., & Qi, C. (2017). Uniaxial compressive strength and fracture mode of lake ice at moderate strain rates based on a digital speckle correlation method for deformation measurement. *Applied Sciences*, 7(5), 495.

Müller, F., Böhm, A., Herrnring, H., und Polach, F. V. B., & Ehlers, S. (2024). Influence of the ice shape on ice-structure impact loads. *Cold Regions Science and Technology*, 221, 104175.

Pernas-Sánchez, J., Artero-Guerrero, J. A., Varas, D., & López-Puente, J. (2015). Analysis of ice impact process at high velocity. *Experimental Mechanics*, 55, 1669-1679.

Shazly, M., Prakash, V., & Lerch, B. A. (2009). High strain-rate behavior of ice under uniaxial compression. *International Journal of Solids and Structures*, 46(6), 1499-1515.

Wang, X., Li, S., Zhao, Y., Wang, Y., & Yang, Z. (2024). Comparison of Arctic and Antarctic sea ice spatial–temporal changes during 1979–2018. *Journal of Hydrology*, 632, 130966.

Wu, X., & Prakash, V. (2015). Dynamic strength of distill water and lake water ice at high strain rates. *International Journal of Impact Engineering*, 76, 155-165.

Zhang, Y., Liu, R., Yuan, L., Li, J., Jing, C., & Han, D. (2023). Ice breaking by low-velocity impact with a rigid sphere. *International Journal of Impact Engineering*, 182, 104786.